Glutamate Surface Speciation on Amorphous Titanium Dioxide and Hydrous Ferric Oxide

DIMITRI A. SVERJENSKY,*,[†],[‡]
CAROLINE M. JONSSON,[†],[‡]
CHRISTOPHER L. JONSSON,[†],[‡]
HENDERSON J. CLEAVES,[‡] AND
ROBERT M. HAZEN[‡]

Department of Earth & Planetary Sciences, Johns Hopkins University, Baltimore, Maryland 21218, and Geophysical Laboratory, Carnegie Institution of Washington, 5251 Broad Branch Road NW, Washington, DC 20015

Hydrous ferric oxide (HFO) and titanium dioxide exhibit similar strong attachment of many adsorbates including biomolecules. Using surface complexation modeling, we have integrated published adsorption data for glutamate on HFO over a range of pH and surface coverage with published *in situ* ATR-FTIR studies of glutamate speciation on amorphous titanium dioxide. The results indicate that glutamate adsorbs on HFO as a deprotonated divalent anion at pH 3–5 and 0.2 μmol·m^{-2} in the form of chelating-monodentate and bridging-bidentate species attached to the surface through three or four of the carboxylate oxygens, respectively. The amine group may interact weakly with the surface. However, at similar pH values and higher surface coverages, glutamate adsorbs mainly as a monovalent or divalent anion chelated to the surface by the γ-carboxylate group. In this configuration the α-carboxylate and amine groups might be free to interact above the surface with the free ends of adjacent glutamates, suggesting a possible mechanism for chiral self-organization and peptide bond formation.

Introduction

The attachment of aqueous amino acids to mineral surfaces is of fundamental interest in a variety of natural and artificial processes ranging from biomineralization (*1, 2*) to the viability of implants of metallic titanium in the human body (*3*). Amino acid–mineral surface interactions may also have played a central role in life's origins, either in determining chiral selection of left-handed amino acids in proteins or in facilitating the formation of peptide bonds (*4*). However, very little is known about the way amino acids attach to even the simplest mineral surfaces in water. The adsorption behavior as a function of environmental parameters such as pH, ionic strength, type of electrolyte, and surface coverage is poorly known, because few adsorption studies carried out under well-defined conditions exist (*5-10*). In addition, very few *in situ* ATR-FTIR spectroscopic studies have been carried out

(*10-13*). Given this lack of data, there have been only a handful of surface complexation models of amino acid adsorption (*7-9*).

In contrast to the lack of information about the amino acid–mineral–water interface, considerable progress has been made in applying *in situ* ATR-FTIR spectroscopic and X-ray studies to investigate the way oxyanions attach to oxide surfaces. Results are available for the inorganic species sulfate, selenate, arsenite, arsenate, phosphate, and borate (*14-22*), the monocarboxylates acetate and benzoate (*23*), and the dicarboxylates oxalate, succinate, maleate, and phthalate (*24-27*). One unambiguous result of these studies is that there are generally two or more surface-bound oxyanion species whose proportions vary systematically with changes in environmental parameters. Another interesting result is that oxyanions often adsorb as partially or completely deprotonated species at pH values where the aqueous oxyanion is protonated. Integration of the spectroscopic results with the results of adsorption and proton surface titration experiments, along with the results of molecular calculations has recently become possible with surface complexation models (*28-30*). Equilibrium binding constants based on internally consistent standard states has enabled direct comparison of the binding strength of a given oxyanion on different oxides (*31-33*). Such comparisons suggest that oxyanions bind equally strongly to freshly precipitated hydrous ferric oxide (HFO) and titanium dioxide. Therefore it should be possible to apply the same speciation information to both oxides.

The amino acids most similar to dicarboxylate oxyanions are aspartate and glutamate. For these ions, an *in situ* ATR-FTIR spectroscopic study (*13*) inferred at least three modes of surface attachment of glutamate on amorphous titanium dioxide (Figure 1). In the present study, we use these ATR-FTIR results as a guide to interpret published glutamate adsorption experiments for HFO (*5*). We do this by developing a quantitative surface complexation model of the chemical reactions at the iron oxide–water–electrolyte interface using the approach developed in ref (*30*). We find that the same three surface species of glutamate can describe adsorption on titanium dioxide and HFO. The proportions of these species vary according to the pH and the amount of glutamate, but are predicted to show little variation with ionic strength. Interestingly, at high concentrations of glutamate, our model predicts that the elongate glutamate molecules attach by the γ-carboxylate end only and "stand up" on the surface. The other ends of the glutamate molecules, containing the α-carboxylate and amine groups, point away from the surface and are potentially able to interact with the free ends of adjacent glutamates. This alignment could provide a mechanism for chiral self-organization and peptide bond formation.

Experimental Section

Spectroscopic Evidence of Glutamate Surface Speciation.
The *in situ* ATR-FTIR spectroscopic study of glutamate on amorphous titanium dioxide (*13*) emphasized surface speciation changes as functions of pH and glutamate concentration. No changes as a function of ionic strength were reported. Bulk adsorption data for aspartate on titanium dioxide showed no dependence on ionic strength (*7*). We have summarized the principle changes inferred in the ATR-FTIR study in Figure 2. We used pH and aqueous glutamate concentration as the axis variables in Figure 2 because these were the experimental parameters. Conversion of the aqueous glutamate concentration to surface coverages is not possible except in a qualitative sense, because the surface area of the

* Corresponding author tel: 410-516-8568; fax: 410-516-7933; e-mail: sver@jhu.edu.
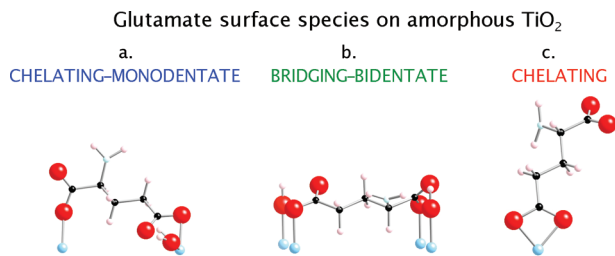† Johns Hopkins University.
‡ Carnegie Institution of Washington.

Glutamate surface species on amorphous TiO$_2$

a. CHELATING–MONODENTATE   b. BRIDGING–BIDENTATE   c. CHELATING

FIGURE 1. Surface species inferred from ATR-FTIR study of glutamate attached to the surface titanium ions of amorphous TiO$_2$ (*13*). These surface species are also consistent with the surface complexation calculations reported in the present study. Large spheres refer to oxygen, small filled spheres refer to carbon, small pale spheres refer to hydrogen or nitrogen, and the lowermost spheres refer to titanium. (a) Chelating-monodentate species with three points of attachment involving two inner-sphere Ti—O—C bonds and one Ti—OH$_2$...O—C hydrogen bond. One C=O group of the α-carboxylate is free. (b) Bridging-bidentate species with four points of attachment involving two inner-sphere Ti—O—C bonds and two Ti—OH...O—C hydrogen bonds. (c) Chelating species with two points of attachment involving two inner-sphere Ti—O—C bonds to a single titanium ion.
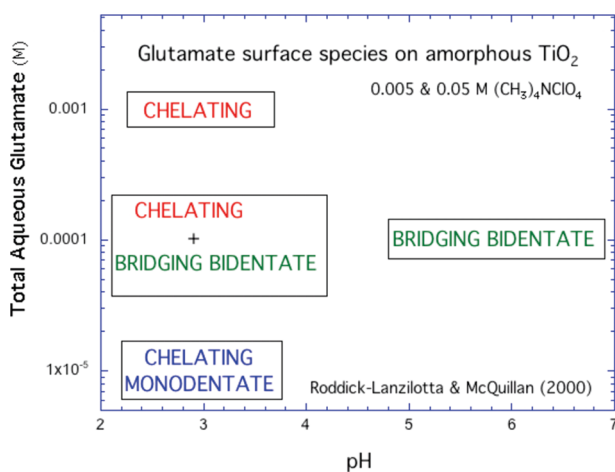

FIGURE 2. Summary of the glutamate surface speciation inferred from ATR-FTIR spectroscopic results.

amorphous titanium dioxide is not known and the solid concentration is only known approximately.

It is important to emphasize that Figures 1 and 2 illustrate our interpretation of the discussion in the ATR-FTIR study. Additional modes of surface attachment were also mentioned as possibilities. Our representation in Figure 2 is an attempt to summarize the speciation inferred in the ATR-FTIR study in terms of the smallest set of species consistent with their discussion and the surface complexation calculations discussed below. For example, we infer a combination of inner-sphere (Ti—O—C) bonds and hydrogen bonds (TiOH...O—C) in Figure 1a and b, whereas only species involving inner-sphere bonds were depicted in the ATR-FTIR study. Such differences may be difficult to determine from either FTIR spectroscopic experiments or molecular calculations (*24*). Consequently, we relied on the surface complexation modeling to make a choice. Figures 1 and 2 do, however, preserve the major features of the glutamate attachment modes inferred previously (*13*).

Figure 2 illustrates the two principle changes in glutamate surface speciation inferred in the ATR-FTIR study. The first is a speciation change as a function of total glutamate concentration at pH = 3. At the lowest glutamate concentrations (1 × 10^{-5} M), a chelating-monodentate species was inferred by the latter authors. Here there are three points of

attachment of the glutamate to the surface (Figure 1a), i.e., the glutamate molecule can be thought of as "lying down" on the surface. The γ-carboxylate is chelated to a single Ti by a hydrogen bond (TiOH$_2$$^+$...O—C) and a Ti—O—C bond. The α-carboxylate is monodentate, with only one O attached to a Ti through a Ti—O—C bond while the other oxygen forms a C=O entity. The state of protonation of this species in Figure 1a represents our best estimate for a species of this type based on the surface complexation calculations. At the highest glutamate concentrations in Figure 2 (1 × 10^{-3} M), a chelating species was inferred (Figure 1c). Here the γ-carboxylate chelates to a single Ti either with two Ti—O—C bonds (as shown in the figure) or with one Ti—O—C bond and one TiOH...O—C hydrogen bond. We could not distinguish between these two possibilities in our surface complexation calculations. In both possibilities, the α-carboxylate and amine groups are pointing away from the surface, i.e., the glutamate molecule is "standing up" on the surface. However, in the species shown in Figure 1c the amine group is deprotonated, whereas in the other possible mode it is protonated. Interaction of the γ-carboxylate with an alumina surface, also at high surface coverage, has previously been suggested (*10*) although only a single surface coverage was reported. It should also be noted that no definitive information on the state of protonation of the amine group in the adsorbed glutamate was reported in ref (*13*) because the adsorption bands are so weak.

At pH = 3 and intermediate glutamate concentrations (1 × 10^{-4} M) in Figure 2 the chelating attachment mode is accompanied by at least one other surface species, possibly a bridging-bidentate species. Here there are four points of attachment of the glutamate to the surface (Figure 1b). The glutamate molecule can again be thought of as "lying down" on the surface. Both carboxylate groups are bound to the surface in the same way: one oxygen is coordinated directly to a Ti and the other is coordinated through a hydrogen bond to a different Ti. The state of protonation of this species in Figure 1b represents our best estimate for a species of this type based on the surface complexation calculations. For example, a species in which all four oxygens of the carboxylate groups were directly coordinated to four different Ti atoms could not fit the adsorption data satisfactorily.

Overall, the major glutamate surface speciation change at pH = 3 as a function of increasing glutamate concentration is a transition from glutamate "lying down" at the lowest concentration to "standing up" at the highest concentration. This change may be attributable to surface crowding at progressively higher glutamate concentrations (*13*). The second principle change in speciation emphasized by the latter authors is a change as a function of pH. At the intermediate glutamate concentration and pH = 3 in Figure 2, the bridging-bidentate species is just one of at least two surface glutamate species. However, at higher pH values approaching neutrality, it was reported to be the predominant species.

The existence of multiple surface species of glutamate on amorphous titanium dioxide and the systematic changes as a function of environmental parameters are both features of the amino acid—mineral—water interface that are similar to the more extensive results obtained for both inorganic and organic oxyanions. Integration of these features into a surface complexation model permits application of the spectroscopic results to the adsorption of glutamate on other similar solids over a wide range of environmental conditions.

Surface Complexation Model of Glutamate on HFO. The approach used in the present study builds on the predictive single-site triple-layer model and associated crystal chemical and Born solvation theory referred to as the extended triple-layer model or ETLM (*34-36*). Recent theoretical advances in the application of the ETLM to oxyanion adsorption on

TABLE 1. Aqueous Glutamate Properties [a], HFO Characteristics[b], and Extended Triple-Layer Model Parameters for Proton, Electrolyte, and Glutamate Adsorption on Hydrous Ferric Oxide

Name	Reaction	logK
	$Glu^{2-} + H^+ = HGlu^-$	9.96
	$HGlu^- + H^+ = H_2Glu^0$	4.30
	$H_2Glu^0 + H^+ = H_3Glu^+$	2.16
	$HGlu^- + NO_3^- + 2H^+ = H_3(Glu)NO_3^0$	5.3
	$HGlu^- + Na^+ = Na(HGlu)^0$	-0.3
	$HGlu^- + Na^+ = NaGlu^- + H^+$	-9.6
	Hypothetical 1.0 m standard state	
$\log K_1^0$	$>SOH + H^+ = >SOH_2^+$	3.7
$\log K_2^0$	$>SO^- + H^+ = >SOH$	12.1
$\log {}^*K_{M^+}^0$	$>SOH + M^+ = >SO^- \_M^+ + H^+$	-7.8
$\log {}^*K_{L^-}^0$	$>SOH + H^+ + L^- = >SOH_2^+ \_L^-$	8.2
$\log {}^*K_{(>Fe)>Fe(OH_2^+)Glu}^0$	$>FeOH + >Fe(OH)_2 + 2H^+ + HGlu^- = >Fe>Fe(OH_2^+)Glu + 2H_2O$	22.0
$\log {}^*K_{(>FeOH)_2(>Fe)Glu}^0$	$4>FeOH + H^+ + HGlu^- = (>FeOH)_2>Fe_2Glu + 2H_2O$	20.0
$\log {}^*K_{>FeO_2Glu}^0$	$>Fe(OH)_2 + H^+ + HGlu^- = >FeGlu + 2H_2O$	7.8
	Site-occupancy standard states[c]	
$\log K_{(>Fe)>Fe(OH_2^+)Glu}^\theta$	$>FeOH_2^+ + >Fe(OH_2^+)_2 + HGlu^- = >Fe>Fe(OH_2^+)Glu + H^+ + 2H_2O$	10.4
$\log K_{(>FeOH)_2(>Fe)Glu}^\theta$	$2>FeOH + 2>FeOH_2^+ + HGlu^- = (>FeOH)_2>Fe_2Glu + 2H_2O$	18.1
$\log K_{>FeO_2Glu}^\theta$	$>Fe(OH_2^+)_2 + HGlu^- = >FeGlu + H^+ + 2H_2O$	4.06

[a] Protonation constants from ref (40); electrolyte ion pair constants assumed to be the same as for aspartate given by ref (41). [b] HFO properties are $N_s = 3.8$ sites·nm^{-2}, $A_s = 600$ m^2·g^{-1}, $C_1 = 100$ μF·cm^{-2}, pH$_{ZPC}$ = 7.9, ΔpK_n^θ = 5.6, log K_1^θ = 5.1, log K_2^θ = 10.7, log $K_{M^+}^\theta$ = 4.3, log $K_{L^-}^\theta$ = 4.5 (32). [c] Equilibrium constants relative to site-occupancy standard states were also written relative to charged surface sites calculated using the following equations:

$$\log K_{(>Fe)(>Fe(OH_2^+)Glu}^\theta = \log^* K_{(>Fe)(>Fe(OH_2^+)Glu}^0 + \log \frac{(N_sA_s)^2C_s}{100} - 3pH_{ZPC} + \frac{3}{2}\Delta pK_n^\theta$$

$$\log K_{(>FeOH)_2(>Fe)_2Glu}^\theta = \log^* K_{(>FeOH)_2(>Fe)_2Glu}^0 + \log \frac{(N_sA_s)^4C_s^3}{100} - 2pH_{ZPC} + \Delta pK_n^\theta$$

$$\log K_{>FeO_2Glu}^\theta = \log^* K_{>FeO_2Glu}^0 + \log \frac{(N_sA_s)}{100} - pH_{ZPC} + \frac{\Delta pK_n^\theta}{2}$$
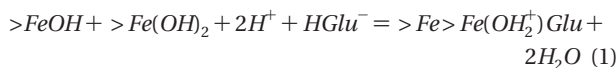
oxide surfaces (30, 33) have emphasized the role of water dipoles during adsorption and indicated the magnitude of this effect. These advances have facilitated incorporation of the nature of surface species established by spectroscopic studies into surface complexation calculations. In turn this modeling has enabled prediction of surface speciation as a function of environmental parameters consistent with spectroscopically established trends. We apply the ETLM here to the adsorption of glutamate on HFO (5). We investigate the applicability of the three surface species deduced above for glutamate on amorphous titanium dioxide to the adsorption of glutamate on HFO. In particular the level of protonation of the surface species are determined from the stoichiometry of the reactions formulated through iterative application of the surface complexation calculations to the bulk adsorption data for HFO.

Surface chemical studies of HFO (37, 38) established that freshly precipitated HFO aged for 4 h is a reliable solid for use in surface chemistry experiments. We have previously analyzed the proton surface charge and sulfate and selenate adsorption data measured by Davis and Leckie for this solid (32). The surface chemical characteristics of the HFO, i.e., the BET surface area and the surface protonation and electrolyte adsorption equilibrium constants, capacitance, and site density, are given in Table 1. X-ray diffraction studies of freshly precipitated HFO have established that it is the mineral ferrihydrite, whose crystal structure has recently been determined (39) yielding a formula of Fe$_{10}$O$_{14}$(OH)$_2$. The latter corresponds to 81.6 g·mole^{-1} of Fe, which we have used in our surface complexation calculations to convert the 0.001 M concentration of Fe in the glutamate adsorption
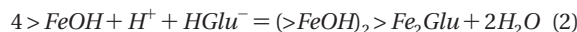
experiments to a solid concentration of HFO in g·L^{-1}. Aqueous protonation of glutamate was treated using equilibrium constants taken from the NIST compilation (40). Electrolyte ion-pairing with glutamate was approximated by assuming that it was the same as literature values for aspartate (41). The equilibrium constants for aqueous glutamate are summarized in Table 1. Aqueous activity coefficients were calculated using the extended Debye–Hückel equation (42), using previously described electrolyte characteristics (43).

Three surface complexation reactions, corresponding to the formation of the species depicted in Figure 1a, b, and c, were found to be consistent with the adsorption data plotted in Figure 3a. The reactions are represented as follows:
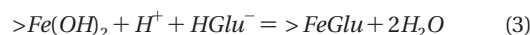
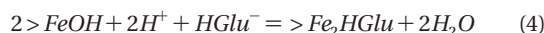Chelating-monodentate species (Figure 1a)

$$>FeOH + >Fe(OH)_2 + 2H^+ + HGlu^- = >Fe>Fe(OH_2^+)Glu + 2H_2O \quad (1)$$

Bridging-bindentate species (Figure 1b)

$$4>FeOH + H^+ + HGlu^- = (>FeOH)_2>Fe_2Glu + 2H_2O \quad (2)$$

Chelating species (Figure 1c)

$$>Fe(OH)_2 + H^+ + HGlu^- = >FeGlu + 2H_2O \quad (3)$$
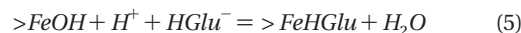
It should be noted that writing the species $>FeOH$ and $>Fe(OH)_2$ in eqs 1 and 3 implies a two-site model. However, eqs 1 and 3 are computationally almost identical to the reactions

$$2>FeOH + 2H^+ + HGlu^- = >Fe_2HGlu + 2H_2O \quad (4)$$

and

$$>FeOH + H^+ + HGlu^- = >FeHGlu + H_2O \quad (5)$$

respectively, which are true single-site reactions. Similar representations of $>FeOH$ and $>Fe(OH)_2$ have been used previously (44). As noted above (see also Figure 1), eqs 1, 2, and 3 refer to the completely deprotonated form of glutamate. This is similar to results for many inorganic and organic oxyanions which adsorb as partially or completely deprotonated species at pH values where the aqueous oxyanion is protonated.

The reactions in eqs 1, 2, and 3 correspond to the equilibrium constants

$$\log^* K_{(>Fe)(>Fe(OH_2^+)Glu}^\theta = \frac{a_{(>Fe)(>Fe(OH_2^+)Glu}a_{H_2O}^2}{a_{>FeOH}a_{>Fe(OH)_2}a_{H^+}^2 a_{HGlu^-}}10^{\frac{F\Delta\Psi_{r,1}}{2.303RT}} \quad (6)$$

$$\log^* K_{(>FeOH)_2(>Fe)_2Glu}^\theta = \frac{a_{(>FeOH)_2(>Fe)_2Glu}a_{H_2O}^2}{a_{>FeOH}^4 a_{H^+}a_{HGlu^-}}10^{\frac{F\Delta\Psi_{r,2}}{2.303RT}} \quad (7)$$

$$\log^* K_{FeGlu}^\theta = \frac{a_{>FeGlu}a_{H_2O}^2}{a_{>Fe(OH)_2}a_{H^+}a_{HGlu^-}}10^{\frac{F\Delta\Psi_{r,3}}{2.303RT}} \quad (8)$$

where the superscripts "*" and "θ" refer to reactions written relative to $>FeOH$, and to site-occupancy standard states (34), respectively. The terms involving $\Delta\Psi_{r,1}$, $\Delta\Psi_{r,2}$ and $\Delta\Psi_{r,3}$ in eqs 6, 7, and 8 represent the electrical work involved in the reaction. In the ETLM, the electrical work includes contributions not only for the ions going on or off the surface, but also for the water dipoles coming off the surface in eqs 1, 2, and 3. The latter contribution to $\Delta\Psi_r$ is $-n_{H_2O}(\Psi_0 - \Psi_\beta)$, where n_{H_2O} represents the number of moles of water on the right side of the reaction. In eqs 1, 2, and 3, $n_{H_2O} = 2$, which results in $\Delta\Psi_{r,1} = \Psi_0$ and $\Delta\Psi_{r,2} = \Delta\Psi_{r,3} = 0$.

The regression calculations discussed below generated values of the equilibrium constants for glutamate adsorption
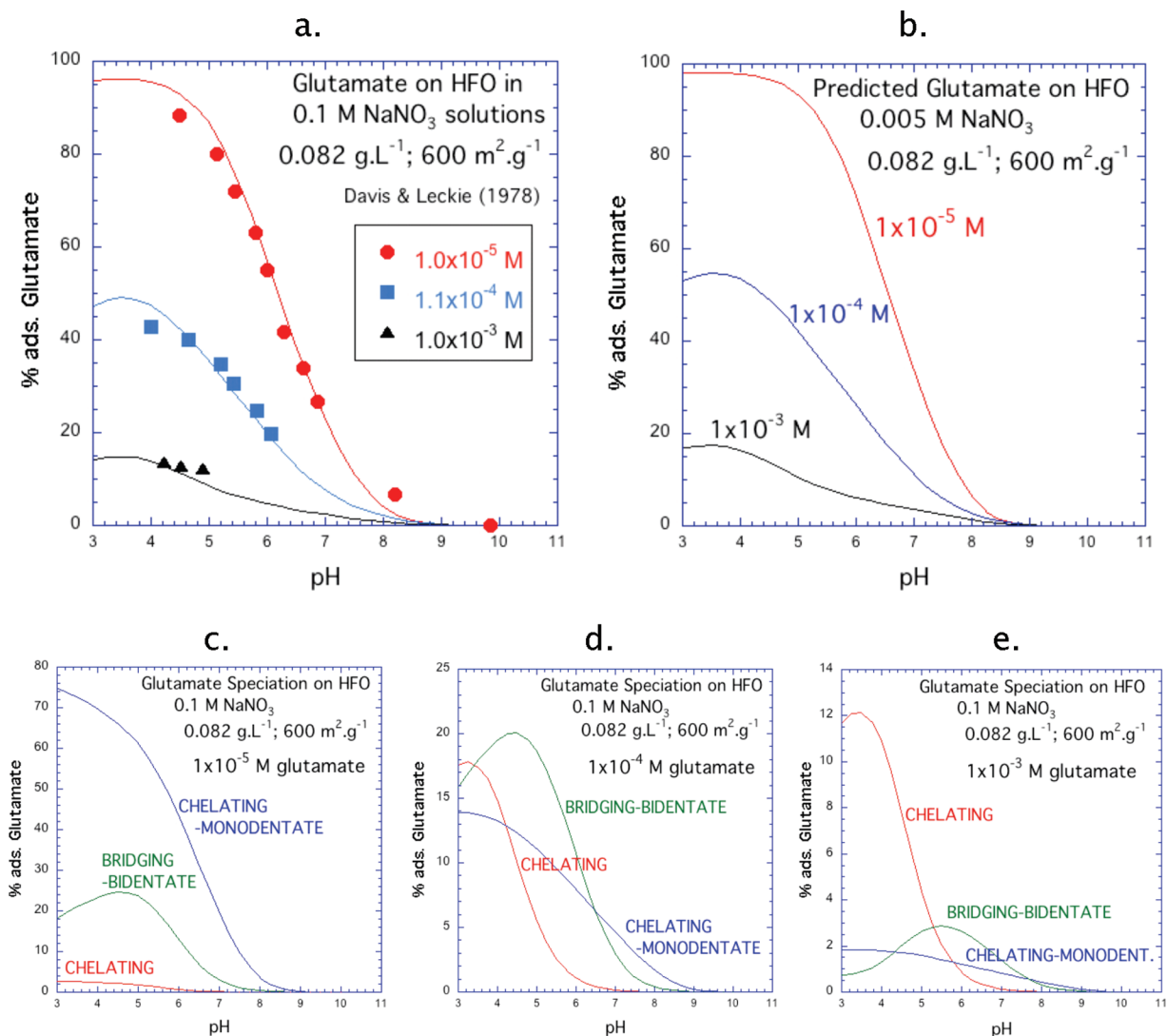
FIGURE 3. Surface complexation model calculations for glutamate on HFO. (a) Data points from ref (5). Solid curves represent a model fit to the data using the surface species in Figure 1. (b) Predicted adsorption at 0.005 M NaNO₃. (c)−(e) Predicted surface speciation as a function of pH and surface coverage for comparison with spectroscopic results in Figure 2.

for the jth surface species represented by $\log^*K^0_j$ in Table 1. The superscript "0" represents the hypothetical 1.0 M standard state (34). These values were converted to values of $\log K^\theta_j$ referring to site-occupancy standard states and referenced to $>SO^-$ using equations and the values of N_s (site density), A_s (BET surface area), pH_{ZPC}, and ΔpK^θ_n given in Table 1. The values of $\log K^\theta_j$ in Table 1 are independent of the individual sample characteristics. Consequently, values of $\log K^\theta_j$ are useful for comparing the binding of glutamate on different oxides.

Adsorption data for glutamate on HFO in 0.1 M NaNO₃ solutions at three total glutamate concentrations are represented by the symbols in Figure 3a. The solid curves in the figures represent regression calculations using the reactions in eqs 1, 2, and 3. The data sets are noteworthy for the strong adsorption at pH values less than about 7 and for the strong dependence on glutamate concentration (i.e., surface coverage). The assessment of uncertainties in experimental adsorption studies is often not provided. However, for anion uptake experiments, uncertainties are typically largest at the lowest percentages adsorbed and may be of the order of ± 5−10% adsorbed (7). The calculated curves in Figure 3a show relatively small discrepancies with the experimental data within this uncertainty. Clearly, the surface species indicated by ATR-FTIR spectroscopy for glutamate on titanium dioxide

can be applied to describe glutamate adsorption on HFO as a function of pH and surface coverage. Many other surface complexation reaction stoichiometries were tested, but did not satisfactorily account for the adsorption data and preserve consistency with the spectroscopic results. Our equilibrium constants for glutamate adsorption were also tested by predicting the ionic strength dependence of glutamate adsorption and the trends of surface speciation with pH and surface coverage.

Although the ionic strength dependence of glutamate adsorption on HFO was not reported, the adsorption of aspartate on titanium dioxide shows no ionic strength dependence (7). Assuming, as a first approximation, that aspartate and glutamate have similar behavior, we might expect that glutamate adsorption will also not show a significant ionic strength dependence. Predicted adsorption curves for glutamate in 0.005 M NaNO₃ solutions are shown in Figure 3b, where it can be seen that they are almost identical to the curves in Figure 3a.

Additional tests of the ETLM for glutamate adsorption on HFO can be made by predicting the surface speciation changes as functions of surface coverage and pH. Predicted model speciation curves for three surface coverages are shown in Figure 3c, d, and e. The curves in this figure can be compared to the trends in Figure 2. At pH = 3, it can be

seen in Figure 3c, d, and e that the predominant species is predicted to change with increasing surface coverage from the chelating-monodentate type to the chelating type. The same change is evident in Figure 2. At pH 3 and the intermediate surface coverage (Figure 3d), the two most abundant surface complexes are predicted to be the bridging-bidentate and the chelating types, which also agrees with the spectroscopic results. As pH increases to between 5 and 7 at the two highest surface coverages (Figures 3d and e), it can be seen that the bridging-bidentate complex is predicted to become more important, even dominant, which again agrees qualitatively with Figure 2. More detailed comparisons would be possible if the exact surface coverages for the spectroscopic data were known. However, the predicted speciation changes for glutamate on HFO are qualitatively consistent with the trends inferred in the spectroscopic study.

Discussion

The calculations described above provide a preliminary picture of the adsorption of glutamate on oxide surfaces by integrating *in situ* spectroscopic results with bulk adsorption data. We have established that the same three surface species of glutamate can describe adsorption on amorphous titanium dioxide and HFO. The surface speciation is predicted to vary according to the pH and the amount of glutamate in ways that are qualitatively consistent with trends inferred from the spectroscopic study. In addition, the bulk adsorption is predicted to show little variation with ionic strength, which is consistent with independent data for aspartate adsorption on titanium dioxide. Both of these results are of broader interest.

The changes in glutamate surface speciation described above may have implications for origin of life studies. At low pH and at low and intermediate surface coverages, the ATR-FTIR study (*13*) and our model indicate that, together, the chelating-monodentate and bridging-bidentate species (Figure 1a and b) are predominant. Both species can be thought of as glutamate molecules essentially "lying down" on the surface. However, at low pH and the highest surface coverages, the chelating species (Figure 1c) predominates. In this picture, the elongate glutamate molecules attach by the γ-carboxylate end only and "stand up" on the surface. The other ends of the glutamate molecules, containing the α-carboxylate and amine groups, point away from the surface and are potentially able to interact with the free ends of adjacent glutamates.

These interactions of adjacent amino acids are of potential interest to models of prebiotic chemistry for at least two reasons. First, such strong interactions could potentially lead to local surface-bound domains of chiral self-organization, as has been observed for clusters of molecules adsorbed to other crystalline surfaces (*45-48*). In addition, the proximity of the amine group from one glutamate to the α-carboxylate group of an adjacent amino acid might promote peptide bond formation. Thus adsorption of amino acids onto mineral surfaces could promote both the selection and synthesis of homochiral prebiotic oligomers (*4*).

The apparent lack of variation of adsorption with ionic strength for glutamate and aspartate on oxide minerals provides a contrast with results for oxyanions in general, and dicarboxylate anions in particular. The latter typically show a significant dependence of adsorption on ionic strength. In our surface complexation model for glutamate, the predicted lack of ionic strength dependence is a consequence of the reactions used. Specifically, the three electrostatic factors in eqs 6, 7, and 8), i.e., $\Delta\Psi_{n1} = \Psi_0$ and $\Delta\Psi_{n2} = \Delta\Psi_{n3} = 0$, are either zero or only weakly dependent on ionic strength. In turn, this is a consequence of the number of water molecules desorbing from the surface in eqs 1, 2,

and 3. In contrast, dicarboxylate anions, such as succinate, fumarate, maleate on alumina, and phthalate on hematite (*24-49*), adsorb with a strong dependence on ionic strength which may result from a combination of a different number of water molecules desorbing and the existence of outer-sphere surface species. It therefore appears that there are significant differences in the behavior of the acidic amino acids and dicarboxylate anions on a variety of oxide surfaces.

Literature Cited

(1) De Yoreo, J. J.; Wierzbicki, A.; Dove, P. M. New insights into mechanisms of biomolecular control on growth of inorganic crystals. *Cryst. Eng. Commun.* **2007**, *9*, 1144–1152.

(2) Elhadj, S.; Salter, E. A.; Wierzbicki, A.; De Yoreo, J. J.; Han, K. N.; Dove, P. M. Peptide controls on calcite mineralization: Polyaspartate chain length affects growth kinetics and acts as a stereochemical switch on morphology. *Cryst. Growth Des.* **2006**, *6*, 197–201.

(3) Kasemo, B. Biological surface science. *Surf. Sci.* **2002**, *500*, 656–677.

(4) Hazen, R. M. Mineral surfaces and the prebiotic selection and organization of biomolecules. *Am. Mineral.* **2005**, *91*, 1715–1729.

(5) Davis, J. A.; Leckie, J. O. Effect of adsorbed complexing ligands on trace metal uptake by hydrous oxides. *Environ. Sci. Technol.* **1978**, *12*, 1309–1315.

(6) Ballion, D.; Jaffrezic-Renault, N. Study of the uptake of inorganic ions and organic acids at the α-alumina-electrolyte interface in a colloidal system by radiochemical techniques and micro-electrophoresis. *J. Radioanal. Nucl. Chem.* **1985**, *92*, 133–150.

(7) Giacomelli, C. E.; Avena, M. J.; De Pauli, C. P. Aspartic acid adsorption onto TiO_2 particles surface. Experimental data and model calculations. *Langmuir* **1995**, *11*, 3483–3490.

(8) Vlasova, N. N. Adsorption of copper-amino acid complexes on the surface of highly dispersed silica. *Colloid J.* **2005**, *67*, 537–541.

(9) Vlasova, N. N.; Golovkova, L. P. The adsorption of amino acids on the surface of highly dispersed silica. *Colloid J.* **2004**, *66*, 657–662.

(10) Fitts, J. P.; Persson, P.; Brown, G. E. J.; Parks, G. A. Structure and bonding of Cu(II)-glutamate complexes at the γ-Al_2O_3-water interface. *J. Colloid Interface Sci.* **1999**, *220*, 133–147.

(11) Roddick-Lanzilotta, A. D.; Connor, P. A.; McQuillan, A. J. An in situ infrared spectroscopic study of the adsorption of lysine to TiO_2 from an aqueous solution. *Langmuir* **1998**, *14*, 6479–6484.

(12) Roddick-Lanzilotta, A. D.; McQuillan, A. J. An in situ infrared spectroscopic investigation of lysine peptide and polylysine adsorption to TiO_2 from aqueous solutions. *J. Colloid Interface Sci.* **1999**, *217*, 194–202.

(13) Roddick-Lanzilotta, A. D.; McQuillan, A. J. An in situ infrared spectroscopic study of glutamic acid and of aspartic acid adsorbed on TiO_2: Implications for the biocompatibility of titanium. *J. Colloid Interface Sci.* **2000**, *227*, 48–54.

(14) Arai, Y.; Elzinga, E.; Sparks, D. L. X-ray absorption spectroscopic investigation of arsenite and arsenate adsorption at the aluminum oxide-water interface. *J. Colloid Interface Sci.* **2001**, *235*, 80–88.

(15) Arai, Y.; Sparks, D. L. ATR-FTIR spectroscopic investigation on phosphate adsorption mechanisms at the ferrihydrite-water interface. *J. Colloid Interface Sci.* **2001**, *241*, 317–326.

(16) Peak, D.; Ford, R. G.; Sparks, D. L. An *in situ* ATR-FTIR investigation of sulfate bonding mechanisms on goethite. *J. Colloid Interface Sci.* **1999**, *218*, 289–299.

(17) Peak, D.; Luther, G. W.; Sparks, D. L. ATR-FTIR spectroscopic studies of boric acid adsorption on hydrous ferric oxide. *Geochim. Cosmochim. Acta* **2003**, *67*, 2551–2560.

(18) Peak, D.; Sparks, D. L. Mechanisms of selenate adsorption on

iron oxides and hydroxides. *Environ. Sci. Technol.* **2002**, *36*, 1460–1466.

(19) Wijnja, H.; Schulthess, C. P. Vibrational spectroscopy study of selenate and sulfate adsorption mechanisms on Fe and Al (Hydr)oxide surfaces. *J. Colloid Interface Sci.* **2000**, *229*, 286–297.

(20) Majzlan, J.; Myneni, S. C. B. Speciation of iron and sulfate in acid waters: Aqueous clusters to mineral precipitates. *Environ. Sci. Technol.* **2005**, *39*, 188–119.

(21) Catalano, J. G.; Zhang, Z.; Fenter, P.; Bedzyk, M. J. Inner-sphere adsorption geometry of Se(IV) at the hematite (100)-water interface. *J. Colloid Interface Sci.* **2006**, *297*, 665–671.

(22) Catalano, J. G.; Zhang, Z.; Park, C.; Fenter, P.; Bedzyk, M. J. Bridging arsenate surface complexes on the hematite (012) surface. *Geochim. Cosmochim. Acta* **2007**, *71*, 1883–1897.

(23) Norén, K.; Persson, P. Adsorption of monocarboxylates at the water/goethite interface: The importance of hydrogen bonding. *Geochim. Cosmochim. Acta* **2007**, *71*, 5717–5730.

(24) Hwang, Y. S.; Liu, J.; Lenhart, J. J.; Hadad, C. M. Surface complexes of pthalic acid at the hematite/water interface. *J. Colloid Interface Sci.* **2007**, *307*, 124–134.

(25) Persson, P.; Axe, K. Adsorption of oxalate and malonate at the water-goethite interface: molecular surface speciation from IR spectroscopy. *Geochim. Cosmochim. Acta* **2005**, *69*, 541–552.

(26) Hug, S. J.; Bahnemann, D. Infrared spectra of oxalate, malonate and succinate adsorbed on the aqueous surface of rutile, anatase and lepidocrocite measured with in situ ATR-FTIR. *J. Electron. Spectrosc. Relat. Phenom.* **2006**, *150*, 208–219.

(27) Johnson, S. B.; Yoon, T. H.; Kokar, B. D.; Brown, G. E., Jr. Adsorption of organic matter at mineral/water interfaces. 2. Outer-sphere adsorption of maleate and implications for dissolution processes. *Langmuir* **2004**, *20*, 4996–5006.

(28) Hiemstra, T.; van Riemsdijk, W. H. Surface structural ion adsorption modeling of competitive binding of oxyanions by metal (hydr)oxides. *J. Colloid Interface Sci.* **1999**, *210*, 182–193.

(29) Hiemstra, T.; Van Riemsdijk, W. H. On the relationship between charge distribution, surface hydration, and the structure of the interface of metal oxides. *J. Colloid Interface Sci.* **2006**, *301*, 1–18.

(30) Sverjensky, D. A.; Fukushi, K. Anion adsorption on oxide surfaces: Inclusion of the water dipole in modeling the electrostatics of ligand exchange. *Environ. Sci. Technol.* **2006**, *40*, 263–271.

(31) Fukushi, K.; Sverjensky, D. A. A predictive model for arsenate adsorption and surface speciation on oxides consistent with spectroscopic and theoretical molecular evidence. *Geochim. Cosmochim. Acta* **2007**, *71*, 3717–3745.

(32) Fukushi, K.; Sverjensky, D. A. A surface complexation model for sulfate and selenate on iron oxides consistent with spectroscopic and theoretical molecular evidence. *Geochim. Cosmochim. Acta* **2007**, *71*, 1–24.

(33) Sverjensky, D. A.; Fukushi, K. A predictive model (ETLM) for As(III) adsorption and surface speciation on oxides consistent with spectroscopic data. *Geochim. Cosmochim. Acta* **2006**, 70.

(34) Sverjensky, D. A. Standard states for the activities of mineral surface-sites and species. *Geochim. Cosmochim. Acta* **2003**, *67*, 17–28.

(35) Sverjensky, D. A. Prediction of surface charge on oxides in salt solutions: revisions for 1:1 (M^+L^-) electrolytes. *Geochim. Cosmochim. Acta* **2005**, *69*, 225–257.

(36) Sverjensky, D. A. Prediction of the speciation of alkaline earths adsorbed on mineral surfaces in salt solutions. *Geochim. Cosmochim. Acta* **2006**, *70*, 2427–2453.

(37) Davis, J. A.; Leckie, J. O. Surface ionization and complexation at the oxide/water interface II. Surface properties of amorphous iron oxyhydroxide and adsorption of metal ions. *J. Colloid Interface Sci.* **1978**, *67*, 90–107.

(38) Dzombak, D. A.; Morel, F. M. M. *Surface Complexation Modeling*; John Wiley and Sons: New York, 1990.

(39) Michel, F. M.; Ehm, L.; Antao, S. M.; Lee, P. L.; Chupas, P. J.; Liu, G.; Strongin, D. R.; Schoonen, M. A. A.; Phillips, B. L.; Parise, J. B. The structure of ferrihydrite, a nanocrystalline material. *Science* **2007**, *316*, 1726–1729.

(40) Smith, R. M.; Martell, A. E. *NIST Critically Selected Stability Constants of Metal Complexes Database*; U. S. Department of Commerce, Technology Administration: Washington, DC, 2004.

(41) De Robertis, A.; De Stefano, C. Salt effects on the protonation of L-histidine and L-aspartic acid: a complex formation model. *Thermochim. Acta* **1991**, *177*, 39–57.

(42) Helgeson, H. C.; Kirkham, D. H.; Flowers, G. C. Theoretical prediction of the thermodynamic behavior of aqueous electrolytes at high pressures and temperatures. IV. Calculation of activity coefficients, osmotic coefficients, and apparent molal and standard and relative partial molal properties to 5 kb and 600 C. *Am. J. Sci.* **1981**, *281*, 1241–1516.

(43) Criscenti, L. J.; Sverjensky, D. A. A single-site model for divalent and heavy metal adsorption over a range of metal concentrations. *J. Colloid Interface Sci.* **2002**, *253*, 329–352.

(44) Arai, Y.; Sparks, D. L.; Davis, J. A. Effects of dissolved carbonate on arsenate adsorption and surface speciation at the hematite-water interface. *Environ. Sci. Technol.* **2004**, *38*, 817–824.

(45) Eckhardt, C. J.; Peachey, N. M.; Swanson, D. R.; Takacs, J. M.; Khan, M. A.; Gong, X.; Kim, J.-H.; Wang, J.; Uphaus, R. A. Separation of chiral phases in monolayer crystals of racemic amphiphiles. *Nature* **1993**, *362*, 614–616.

(46) Lorenzo, M. O.; Baddeley, C. J.; Muryn, C.; Raval, R. Extended surface chirality from supramolecular assemblies of adsorbed molecules. *Nature* **2000**, *404*, 376–379.

(47) Lorenzo, M. O.; Haq, S.; Bertrams, T.; Murray, P.; Raval, R.; Baddeley, C. J. Creating chiral surfaces for enantioselective heterogeneous catalysis: R,R-tartaric acid on Cu(110). *J. Phys. Chem. B* **1999**, *103*, 10661–10669.

(48) Fasel, R.; Parschau, M.; Ernst, K.-H. Amplification of chirality in two-dimensional enantiomorphous lattices. *Nature* **2006**, *439*, 449–452.

(49) Yao, H.; Yeh, H. Fumarate, maleate, and succinate adsorption on hydrous δ-Al$_2$O$_3$. 1. Comparison of the adsorption maxima and their significance. *Langmuir* **1996**, *12*, 2981–2988.